1

Seasonality of Tropical Photosynthesis: A Global Map of Drivers and Comparison to Model Outputs

M. R. Uribe,[1,2] C. A. Sierra,[3] and J. S. Dukes[1,2,4]

[1] Department of Forestry and Natural Resources, Purdue University, West Lafayette, IN.

[2] Purdue Climate Change Research Center, Purdue University, West Lafayette, IN.

[3] Max Planck Institute for Biogeochemistry, Jena, Germany.

[4] Department of Biological Sciences, Purdue University, West Lafayette, IN.

Corresponding author: Maria del Rosario Uribe (uribem@purdue.edu)

Key Points:

- In tropical ecosystems, photosynthetic activity responds strongly to seasonal variation in water and light.

- In most regions, photosynthesis varies with seasonal fluctuations in both resources, but relationships with a single driver are also common.

- The relationship of climate with photosynthetic activity is characterized by water availability and its synchronization with light.

- Land surface models overestimate the extent of positive correlations with water and underestimate those with light.

- The relationships of photosynthetic activity with climate identified from remote sensing data closely agree with global datasets such as VPM and GOSIF.

22 **Abstract**

23 Tropical ecosystems strongly influence Earth's climate and weather patterns. Most tropical
24 ecosystems remain warm year-round; nonetheless, their plants undergo seasonal cycles of carbon
25 and water exchange. Previous research has shown the importance of water and light as drivers of
26 the seasonality of photosynthetic activity in the tropics. Although data are scarce, field-based
27 studies have found that seasonal cycles at a handful of tropical forest sites do not match those in
28 land surface model simulations. A comprehensive understanding and model comparison of how
29 seasonal variations in tropical photosynthetic activity relate to climate is lacking. In this study,
30 we identify the seasonal relationships of precipitation and light availability with satellite-based
31 photosynthetic activity. Three dominant and spatially distinct seasonal relationships emerge
32 between photosynthetic activity and these two environmental drivers: photosynthetic activity that
33 is positively correlated with both drivers (36% of tropical pixels), activity that increases
34 following rain but decreases with light (28%), and activity that increases following bright
35 seasons but decreases with rain (14%). We compare distributions of these observed relationships
36 with those simulated by land surface models. In general, model simulations of gross primary
37 productivity (GPP) overestimate the extent of positive correlations of photosynthetic activity
38 with water and underestimate positive correlations with light. The largest discrepancies between
39 simulations and observations are in the representation of the regions where photosynthetic
40 activity increases with light and decreases with rain. Our clear scheme for representing the
41 relationship between climate and photosynthetic activity can be used to benchmark tropical
42 seasonality of GPP in land models.

43 **Plain Language Summary**

44 Tropical ecosystems strongly influence Earth's atmosphere and climate through their high rates
45 of photosynthesis and transpiration. These rates vary seasonally, but tropical seasonal cycles and
46 their drivers are incompletely characterized. Here, we identify and characterize the three most
47 common relationships between seasonality of photosynthetic activity and two main climatic
48 drivers, water and light. Each type of relationship is associated with specific climate properties.
49 In short, when seasonal cycles of water and light are synchronized, vegetation responds
50 positively to both drivers. When the cycles are not synchronized, drier sites respond positively to
51 water and negatively to light, while wetter sites respond positively to light and negatively to
52 water. Ecosystem models generally lack the mechanisms that lead to this latter relationship. Our
53 improved understanding of these relationships can guide model improvement efforts for tropical
54 ecosystems.

55 **1 Introduction**

56   Tropical ecosystems are sometimes called the "lungs of the planet," because their high
57 photosynthetic rates drive large fluxes of carbon and water. Tropical forests alone account for
58 about 60% of global terrestrial photosynthesis (Mitchard, 2018) and influence precipitation
59 patterns, even at the continental scale (Lawrence & Vandecar, 2015). Collectively, tropical
60 ecosystems disproportionately influence Earth's climate and weather patterns (Malhi et al.,
61 2008).

62   At the intra-annual or seasonal scale, climate patterns determine ecosystems' metabolism,
63 phenological patterns, and vegetation distribution. Ecosystem metabolism, in turn, affects the
64 climate system through photosynthesis and the associated carbon, water, and energy feedbacks to

65 the atmosphere. But this ecosystem-atmosphere interaction is being altered by ongoing changes
66 in the climate system. Forecasting the effects of these climatic changes on tropical ecosystems,
67 and the subsequent consequences for biosphere-atmosphere interactions and climate at regional
68 and global scales requires accurate estimates of current photosynthetic rates in tropical
69 ecosystems and an understanding of their relationship with climate. While photosynthetic rates
70 go through clear and well-understood seasonal cycles in temperate regions, seasonality of
71 photosynthesis in the tropics is less well understood (Wu et al., 2016). Across most ecosystems
72 in these consistently warm regions, both the patterns of seasonality and the drivers of those
73 patterns remain largely uncharacterized (Restrepo-Coupe et al., 2017; Saleska et al., 2003).

74 Marked seasonal patterns in vegetation activity, although sometimes weaker or less
75 defined in comparison to those of the temperate zones, have been observed in both field- and
76 satellite-based measurements in the tropics. Estimates from eddy covariance towers show strong
77 seasonal patterns in net ecosystem exchange and gross primary productivity (GPP) in most sites
78 where data are available (Restrepo-Coupe et al., 2013; Saigusa et al., 2008). Such sites include
79 tropical rain forests and savannas from the Amazon and Asia. Satellite-based measurements of
80 proxies of phenology and photosynthetic activity such as leaf area index (LAI), enhanced
81 vegetation index (EVI) and solar-induced fluorescence (SIF), often show similar seasonal
82 patterns to those observed in the field (Bertani et al., 2017; Bradley et al., 2011a; Guan et al.,
83 2015; Myneni et al., 2007; Xu et al., 2015). These studies demonstrate that seasonality extends
84 across the tropics, with only a small portion of the region not showing any type of seasonality.

85 Land surface models, however, are unable to characterize the observed seasonal cycles,
86 as shown for some specific sites in the Amazon (Restrepo-Coupe et al., 2017). At individual
87 study sites, models simulate either constant GPP or opposite seasonal patterns to the ones
88 observed in the field (Restrepo-Coupe et al., 2017). Yet, these models are a major component of
89 Earth System Models (ESMs) and constitute the main tool scientists currently rely on for future
90 projections of climate, ecosystems and their interrelationship. Models that represent seasonal
91 cycles in the tropics more accurately would be able to estimate how changes in climate
92 seasonality (e.g., timing or length of wet and dry seasons) could affect intra-annual carbon fluxes
93 and, subsequently, the annual carbon budgets of tropical ecosystems (Saleska et al., 2003).
94 Accurate simulation of terrestrial water cycling, including the effects of tropical vegetation on
95 regional to global precipitation patterns, also depends on realistic simulations of photosynthetic
96 activity.

97 In order to accurately represent the seasonality of tropical photosynthetic activity in land
98 surface models, we need to understand the climatic drivers of this seasonality. This involves
99 recognizing how they vary from one region in the tropics to another, and the potential
100 mechanisms and delayed responses involved in the climate-vegetation relationship. Water and
101 light availability are the main drivers of intra-annual variation in vegetation activity in the
102 tropics, and within the region there is wide variation in the responses to these two drivers
103 (Nemani et al., 2003; Seddon et al., 2016). Previous studies attribute the regional differences in
104 vegetation seasonality to water stress (Guan et al., 2015; Wagner et al., 2017). In this sense,
105 photosynthetic activity follows precipitation cycles in drier ecosystems, such as pastures,
106 deciduous forests or degraded forests (Bradley et al., 2011a; Huete et al., 2006). In ecosystems
107 with higher mean annual rainfall or a shorter dry season, like evergreen forests, photosynthetic
108 activity is either less seasonal or more closely associated with light availability (Guan et al.,
109 2015; Nemani et al., 2003). The mechanisms leading to these different vegetation-climate

110 relationships are still being studied and, therefore, are more challenging to represent in land
111 surface models. Moreover, it is common for the relationship of photosynthetic activity with
112 climate to be lagged depending on the climatic factor and vegetation types (Bradley et al., 2011a;
113 D. Wu et al., 2015). Identifying the importance of these lagged correlations in different parts of
114 the tropics can also guide future research and inclusion of underlying mechanisms in models.

115   Despite the large variation in seasonal patterns across the tropical region and the
116 discrepancy found between GPP from field measurements and models, most satellite-based
117 studies of tropical vegetation seasonality have focused on the Amazon basin. Moreover, model
118 performance has only been tested at the site level, also within the Amazon. A global analysis of
119 the drivers of photosynthesis seasonality in the tropics and how they differ in models would
120 unveil large-scale patterns. These discoveries could help experiments and models target weakly
121 represented regions and ecosystems. Here, we investigated how the seasonality of photosynthetic
122 activity across the entire tropical region relates to the two most important regional-level climate
123 drivers; precipitation and radiation. These two variables also provide the main forcing data used
124 by land surface models to simulate most vegetation processes. In contrast to previous studies,
125 rather than identifying a single climate predictor of photosynthetic activity, we sought to
126 characterize its relationship (including direction and magnitude) with both precipitation and
127 radiation. This approach allowed us to identify where in the tropics photosynthesis is positively
128 or negatively associated with each of the two climate drivers, including lagged responses to these
129 drivers. We then identified the climatic variables most commonly associated with each of the
130 various relationships between photosynthesis and the climatic drivers. We expected annual
131 precipitation and variability to explain the relationship with both water and light; for instance,
132 photosynthetic activity in extremely wet regions should be positively correlated with light and
133 negatively correlated with water. In arid regions, photosynthetic activity should be positively
134 correlated with water and negatively correlated with light. In regions that are neither extremely
135 wet nor dry, and with more evenly distributed precipitation throughout the year, we expected
136 photosynthesis to be positively correlated with both water and light. We compared results from
137 remote sensing data with three ecosystem models and two commonly used GPP datasets. We
138 expected the most widespread pattern in these models and datasets to be a positive relationship
139 between photosynthetic activity and water and a negative relationship with light.

140 **2 Materials and Methods**

141   2.1 Climate data

142   Monthly mean precipitation and net radiation were retrieved for the period 2000-2017.
143 Precipitation was obtained from the TRMM (TMPA/3B43) Rainfall V7 product with a spatial
144 resolution of 0.25-degree x 0.25-degree (TRMM, 2011). This product is the best estimate of an
145 algorithm that uses multi-satellite data from two instruments, the Precipitation Radar and the
146 TRMM Microwave Imager (Huffman et al., 2007). Data of incoming shortwave radiation at the
147 surface were obtained from the Energy Balanced and Filled (EBAF) Surface data product
148 Edition 2.8 from the NASA Clouds and the Earth's Radiant Energy System (CERES) experiment
149 at a 1-degree x 1-degree spatial resolution (Loeb et al., 2009). This product is the output of
150 radiative transfer models that use a series of satellite-based observations of top-of-atmosphere
151 radiation and cloud physical and radiative properties to calculate the surface data (Kato et al.,
152 2013).

153   For the characterization of site-specific climate variables, we calculated MAP, mean
154 radiation, mean temperature, mean dry-season length, and precipitation seasonality index. All of
155 the climate variables correspond to the average for the period 2000-2016 for each pixel. MAP
156 and mean radiation were estimated using the datasets above. Mean temperature was estimated for
157 the period of study from the Climatic Research Unit (CRU) Time-Series (TS) Version 4.02 of
158 High-Resolution Gridded Data of Month-by-month Variation in Climate (Harris et al., 2014).
159 The data are in a 0.5 x 0.5-degree grid and are produced based on observational data from
160 national and external meteorological agencies. Dry-season length was obtained from the Rainy
161 and Dry Seasons (RADS) dataset (Bombardi et al., 2019). This dataset uses global gridded daily
162 precipitation datasets to provide several characteristics of precipitation seasonality at 0.25- x
163 0.25-degree spatial resolution. In RADS, seasons are calculated at the local scale based on the
164 accumulated precipitation anomalies of each grid point. Accumulated precipitation anomalies are
165 calculated by comparing daily precipitation against the long-term mean daily precipitation.
166 Calculations of the accumulated anomalies start every year in the dry season, which is estimated
167 as the first minimum harmonic of the precipitation mean annual cycle. The start and end of the
168 wet and dry seasons correspond to inflection points in the accumulated anomalies curve for each
169 cycle. More details of the algorithm and assumptions for these calculations are provided in
170 Bombardi et al. (2019). The precipitation seasonality index was calculated using the Walsh and
171 Lawler equation (Walsh & Lawler, 1981). This index uses the total annual and monthly
172 precipitation for each year within the period of study to characterize the distribution of
173 precipitation throughout the year. Small values indicate less seasonality or equal distribution of
174 the precipitation throughout the year, while higher values indicate higher concentration of
175 precipitation in fewer months.

176   While some areas of the tropics underwent extensive changes in land cover during the
177 study period (Hansen et al., 2013), the models in this study used static land cover data. Because
178 of the contrast between the coarse resolution of the data used here and the fine resolution at
179 which land cover change occurs, we were unable to include this information in our analyses. The
180 effects of land cover change on seasonality of tropical GPP and its response to precipitation and
181 radiation should be examined in future studies.

182   2.2 Satellite-based vegetation data

183   We used three independent datasets to estimate photosynthetic activity in this study. Two
184 of these were satellite-based proxies: Solar Induced Fluorescence (SIF) and the Multi-Angle
185 Implementation of Atmospheric Correction Enhanced Vegetation Index (MAIAC EVI). The
186 third is a remote sensing-derived product based on SIF, known as GOSIF. SIF data came from
187 the GOME2_F data products V27 (Level 3)
188 (https://avdc.gsfc.nasa.gov/pub/data/satellite/MetOp/GOME_F/, accessed on April 2018) (Joiner
189 et al., 2013). This SIF monthly dataset is available at 0.5 x 0.5-degree resolution since 2007. The
190 GOSIF dataset is based on SIF retrievals from OCO-2 in addition to a predictive model and other
191 MODIS remote sensing and meteorological reanalysis datasets
192 (http://data.globalecology.unh.edu/data/GOSIF/, accessed on March 2019) (Li & Xiao, 2019).
193 GOSIF is available monthly at 0.05 x 0.05-degree resolution since 2000. MAIAC EVI was
194 obtained from calibrated and geometrically corrected MODIS Collection 6 Level 1B satellite
195 images (https://portal.nccs.nasa.gov/datashare/maiac/DataRelease/Global-VI-8day-0.05degree/,
196 accessed on September 2018) (A. Lyapustin et al., 2018). The monthly MAIAC EVI product is
197 at 0.05 x 0.05-degree resolution and since 2000.

198   Each of the satellite-based vegetation datasets has advantages and disadvantages. SIF
199 data from the Global Ozone Monitoring Experiment–2 on MetOp-A and -B (GOME 2) should
200 represent photosynthetic activity well, but the temporal period available, from 2007 to 2018 is
201 not an ideal match with available model output, and sensor degradation for GOME-2 has been a
202 concern (Zhang et al., 2018). GOSIF data, developed from Orbiting Carbon Observatory-2
203 (OCO-2) measurements, should approximate the SIF data and covers a longer period, from 2000
204 to 2018. However, the derived data in the GOSIF product are more removed from the direct
205 observations than SIF. MAIAC EVI has a similarly long time series as GOSIF and has been
206 frequently used in tropical ecosystem studies; it has proved to be a better proxy of photosynthetic
207 activity in tropical rainforests than other vegetation indices such as Normalized Difference
208 Vegetation Index (NDVI) or MODIS EVI (Maeda et al., 2016). However, MAIAC EVI is still a
209 vegetation index that estimates vegetation greenness and not photosynthetic activity directly,
210 which is more accurately estimated with SIF (Joiner et al., 2011).

211 Both the SIF and MAIAC EVI datasets have undergone an advanced cloud screening and
212 filtering process, which has made them advantageous to use in the tropics compared to other
213 remote sensing products. In SIF, the main problem of clouds for SIF retrievals is a shielding
214 effect, as, contrary to vegetation indices, the SIF spectral signature is not affected by clouds
215 (Joiner et al., 2014). Therefore, in the SIF dataset used here, cloud filtering is done by removing
216 pixels with effective cloud fractions of >30%. This filter threshold has been proved to maintain
217 spatial and temporal patterns of SIF without altering the sample size and the noise resulting from
218 reduced coverage (Joiner et al., 2013). MAIAC EVI has a sophisticated cloud and aerosol
219 screening correction algorithm. In this later product, pixels with atmospheric contamination are
220 not excluded from the dataset and are not included in our study (A. I. Lyapustin et al., 2012). As
221 part of our time series analysis, we filled data gaps of a maximum of three months using spline
222 interpolation. Pixels with gaps longer than three months in the time series were excluded from
223 the analysis.

224   2.3 Modeled GPP

225   To examine tropical seasonality exhibited in land surface models (LSMs), simulated GPP
226 data were obtained from the TRENDY (Trends and drivers of the regional scale sources and

227   sinks of carbon dioxide) project (Sitch et al., 2015). Most TRENDY models are LSMs
228   commonly coupled with ESMs and used for climate projections. Here, we used TRENDY v5 S2
229   simulations from CLM4.5 (Oleson et al., 2013), JULES (Best et al., 2011), and LPJ-GUESS
230   (Smith et al., 2001). In TRENDY, each model is run globally with different spatial scales and
231   land cover types, but with the same forcing data. Land cover data for the simulations is fixed and
232   provided by each modeling group. In addition to the LSM-simulated GPP, two global GPP
233   products, Fluxcom (Jung & Team, 2016; Tramontana et al., 2016) and VPM (Zhang et al., 2017),
234   were also analyzed. These datasets are derived using field observations, satellite-based
235   measurements, and reanalysis meteorological data, in combination with interpolation or machine
236   learning techniques. The final products are global-scale gridded GPP estimates with long
237   temporal coverage and high spatial resolution (see Table S1 for details).

238   2.4 Data analysis

239   We used time series analysis to identify relationships between climate variables (i.e.,
240   precipitation and radiation) and various estimates of photosynthetic activity (i.e., SIF, GOSIF,
241   MAIAC EVI, and simulated GPP) across the entire tropics. We used cross-correlation function
242   (CCF) analysis (Box et al., 2015), to examine time series of monthly data for each pixel in the
243   tropics (20°N - 20°S) from 2000 to 2015 (except SIF and GOSIF, which were analyzed for 2007-
244   2017 and 2000-2017, respectively). Although the SIF dataset covered different years than the
245   other datasets, the 11 years of SIF data provide a robust basis for our seasonal analyses, and the
246   SIF analyses can be broadly validated with the longer and independent GOSIF dataset. We
247   excluded from all analyses all pixels with a mean EVI of less than 0.1. Those low EVI pixels,
248   which correspond to barren lands or extremely low vegetation cover, were removed to avoid
249   noise in the photosynthetic activity data and the subsequent calculations. Prior to the analysis,
250   each pair of climate and photosynthetic activity variables was resampled to a common spatial
251   resolution in order to enable time series analysis at the pixel level.

252   We used CCF analysis to calculate direct (i.e., same month) and lagged correlations
253   between each climate variable (i.e., independent variable) and each photosynthetic activity
254   variable (i.e., response variable). We quantified lagged correlations between one and four months
255   because a variety of physiological and ecological mechanisms can potentially delay responses of
256   photosynthetic activity to climate (D. Wu et al., 2015). Our lagged correlations analysis allowed
257   us to determine the strongest immediate or lagged correlation between precipitation or radiation
258   and photosynthetic activity.

259   In CCF analysis, temporal dependencies or high autocorrelation in the independent
260   variable (in this case our climate variables) can hide true relationships or suggest false ones.
261   "Prewhitening" can remove autocorrelations by extracting the "white noise" from the
262   independent variable and applying the same transformation to the response variable, in this case,
263   photosynthetic activity (Cryer & Chan, 2008). We used prewhitening to counteract
264   autocorrelation, allowing us to analyze the actual linear relationship between the two time series.
265   The data were pre-whitened by first finding an autoregressive integrated moving average
266   (ARIMA) model for the climate variable time series, and then fitting the photosynthetic activity
267   time series to the ARIMA model. ARIMA models are built using information contained in the
268   time series and are commonly used in forecasting, but in the case of this study, and prewhitening
269   in general, they are used to filter the original series. The CCF was finally performed on the
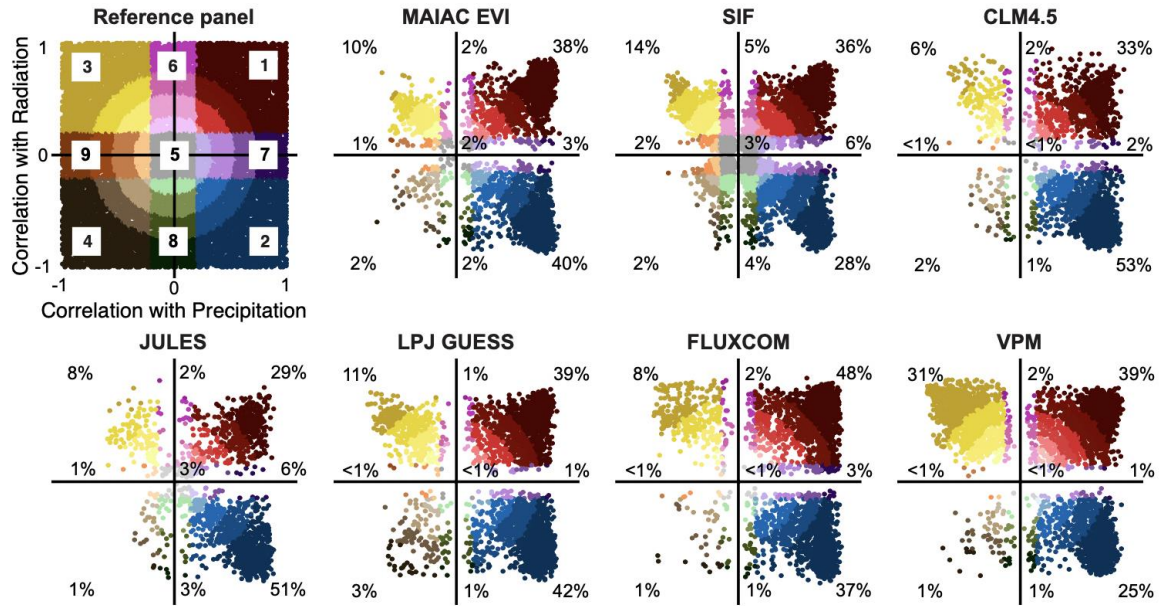270   climate series model residuals and the filtered photosynthetic activity time series (Box et al.,

271 2015; Probst et al., 2012). An example of the CCF analysis is available at
272 https://github.com/rosariouribed/ccf_tropics.

273   Given that precipitation and radiation are two highly correlated variables, we were
274 interested in an analysis that considered the relationship of photosynthetic activity with the two
275 variables individually and in combination. We determined the sign of the maximum direct or
276 lagged correlation coefficient with each variable and then classified the type of relationship
277 based on the signs and strengths of the two coefficients. For instance, photosynthetic activity
278 could be correlated positively with precipitation and negatively with radiation or have a non-
279 significant relationship with precipitation and positive with radiation, and so on (Fig. 1, upper-
280 right reference panel). We created a map for each of the photosynthetic activity datasets showing
281 the type of relationship with climate for each pixel. We assessed the agreement between the
282 results from satellite and model data using the Kappa coefficient (κ) for map agreement (Cohen,
283 1960). The Kappa coefficient compares the agreement between two maps against a hypothetical
284 scenario of randomly assigned values. Coefficients range from -1 to 1, where 0 indicates that the
285 evaluated map is as good as if random values were selected, negative values suggest the map is
286 worse than random values, and positive values suggest the evaluated map matches the reference
287 map better than random values. Values closer to 1 indicate a better agreement between the maps.
288 We also calculated the overall difference (*D*) as a second measurement of agreement of our
289 results. Overall difference has been suggested to provide a more reliable comparison between
290 maps than the Kappa coefficient (Pontius & Santacruz, 2014). Calculations of *D* take into
291 account how well maps agree on (1) the number of pixels classified in each category (i.e.,
292 quantity difference) and (2) the location of the pixels in each category, given the number of
293 pixels in each of the categories (i.e., allocation difference) (Pontius & Santacruz, 2014). Larger
294 *D* values indicate greater disagreement between the maps, either because of under- or
295 overestimation of pixels in the different categories, or because of inaccurate spatial allocation of
296 the pixels in each of the categories. Comparisons between maps were also performed at the
297 biome level in order to identify models' biome-specific shortcomings.

298   We then used the classification of type of relationship and additional climate properties
299 of each pixel to identify climate properties most closely associated with a specific type of
300 relationship. Only the most common types of relationships (i.e., more than 10% of the pixels)
301 were included in the comparison.

302   The additional climate properties included MAP, mean radiation, mean temperature, dry
303 season length, precipitation seasonality index, and the correlation between monthly precipitation
304 and radiation. We used Kruskal-Wallis nonparametric tests (Kruskal & Wallis, 1952) to identify
305 significant differences in the climate properties among the type of relationships. If the Kruskal-
306 Wallis result was significant ($\propto= 0.05$) for a particular variable, we followed up with a pairwise
307 comparison among all types of relationships through the Dunn test with Bonferroni correction
308 (Dunn, 1964). This nonparametric *post hoc* test can be used for independent groups with non-
309 normal distributions and different sizes. All analyses were performed in R 3.4.0 (R Core Team,
310 2017) , including the forecast v8.2 (Hyndman, 2017), TSA v1.01 (Chan & Ripley, 2012), FSA
311 v0.8.22 (Ogle et al., 2018) and diffeR (Pontius Jr. & Santacruz, 2019) packages.

312

313

Fig. 1. Scatterplots showing the maximum correlation coefficient from the CCF analysis for vegetation productivity from each of the datasets with precipitation (x axis) and radiation (y axis). (Top-left/Reference panel): the nine colors and numbers correspond to each of the types of relationships; the rings indicate the strength of the correlation with both drivers (distance from the origin). Regions 1-4 (red, blue, yellow, and brown) indicate significant correlations with both drivers. Region 5 (gray color) indicates non-significant relationships with any driver. Regions 6-9 (pink, purple, green, and orange indicate non-significant correlations with one of the drivers. (Other panels): the numbers indicate the percentage of pixels with the type of relationship where the number is located.

3 Results

3.1 Relationship of photosynthetic activity with precipitation and radiation in satellite data

Based on the direction of the correlations between photosynthetic activity and the two climate drivers, most sites in the tropics can be classified into three categories, with photosynthetic activity that is either (1) positively correlated with both precipitation and radiation, (2) positively correlated with precipitation but negatively correlated with radiation, or (3) positively correlated with radiation but negatively with precipitation (i.e., regions 1, 2 and 3 in Fig. 1 upper-left reference panel). Hereafter, we refer to these three types of relationships as cosynchronous, rain-following and light-following, respectively. For MAIAC EVI and SIF, these three types of relationships together account for 78-88% of tropical pixels, where the cosynchronous pixels correspond to 36-38%, the rain-following 28-40% and the light- following 10-14% of pixels for the two datasets, respectively (Fig. 1). Examples of the seasonal patterns of precipitation, radiation and photosynthetic activity from SIF in pixels from the three main types of relationships are displayed in the Supplementary Materials (Fig. S1). While both datasets agree on the dominance of these three types of relationships, there are some differences between the two datasets in the proportion of pixels that show each of these three dominant types (Fig. 1). In the SIF dataset, more pixels are cosynchronous and light-following and fewer are rain-

341 following than in the MAIAC EVI product. The spatial distribution of the three types of
342 relationships is moderately consistent between the two datasets, with a kappa coefficient of
343 agreement of 0.5 and overall difference of 35.12% (Table 1, Fig. 2). The results from GOSIF
344 agree closely with those from SIF and EVI (κ = 0.52 and 0.65, D= 33.42 and 22.58%,
345 respectively), providing stronger confidence in our results (Fig. S2).
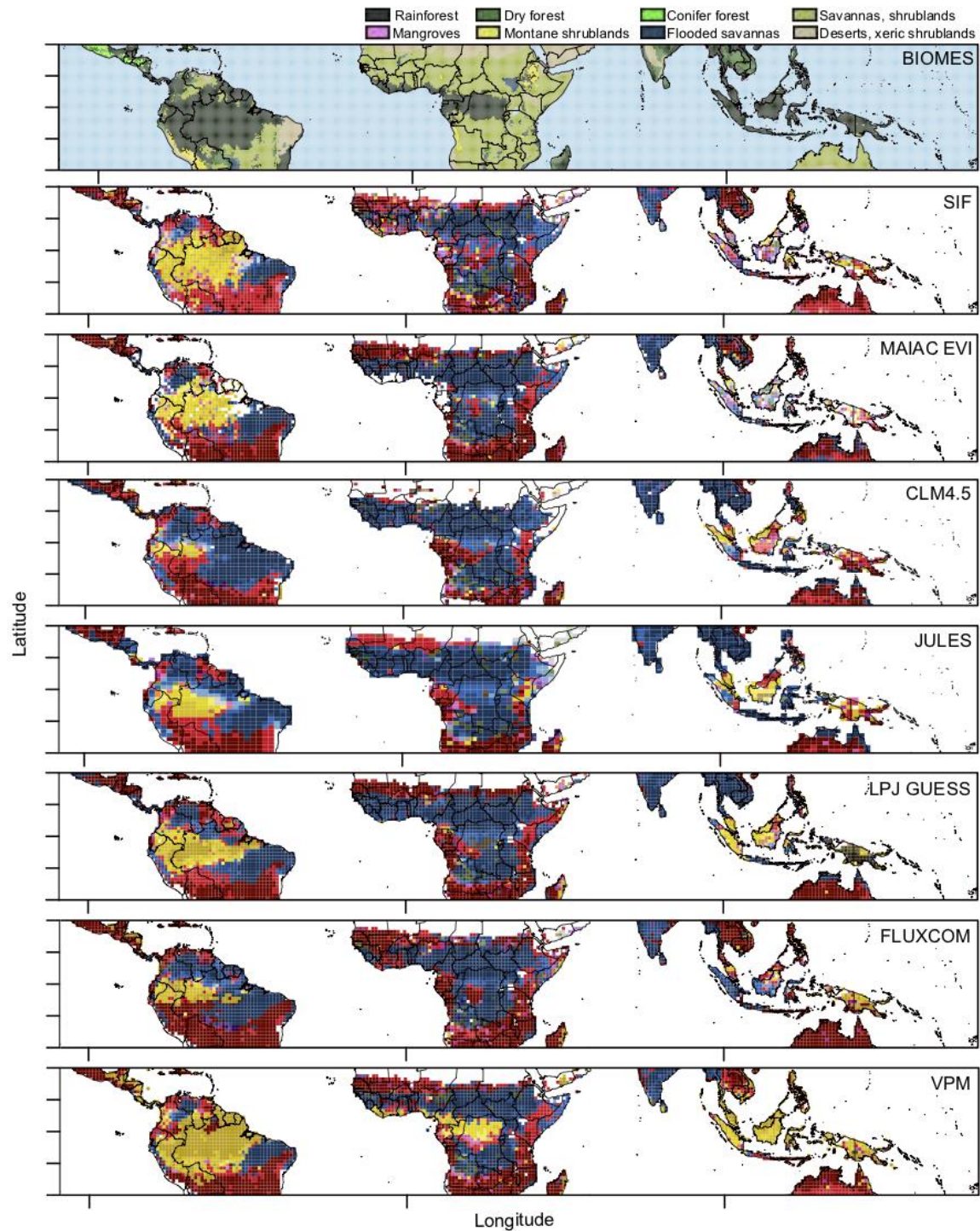
346   Based on the SIF results, cosynchronous pixels (i.e., positive correlations with both
347 precipitation and light) are located across all biomes, but make up the largest fraction (45-86%)
348 of savannas and shrublands, dry broadleaf forests, flooded savannas, montane shrublands, and
349 conifer forest (Fig. S3). The rain-following relationship (28% across all biomes) is most common
350 in savannas and shrublands, dry forests, flooded savannas, and xeric shrublands. Light-following
351 seasonality is mostly clustered in rainforests, specifically those of the Amazon basin and
352 southeast Asia.

353   Other types of relationships are not common (<22% in total), but include negative
354 correlations with both drivers (<3% of pixels) and weak correlations with one (<6% of pixels) or
355 both (<3% of pixels) drivers. For the SIF dataset, these other types of correlations occur mostly
356 in the rainforest in South America, central Africa and southeast Asia. A more detailed look at
357 areas with the weakest relationships shows a prevalence of pixels with very low intra-annual
358 variability in photosynthetic activity. These less distinct types of relationships could also be
359 explained by a higher diversity of vegetation cover or land cover change during the study period.

360   The seasonal peak of photosynthesis most commonly occurred within two months of the
361 seasonal peak of precipitation, while lags with radiation had a much wider range of variation,
362 from 0 to 4 months (Fig. 3, Fig. S4). These lags also varied among the types of relationships. In
363 regions with a cosynchronous relationship, peaks of photosynthesis typically followed peak
364 precipitation by 0-2 months, and peak radiation by 3-4 months (Fig. 3, Fig. S4a). In regions with
365 a rain-following relationship, photosynthetic activity lagged peaks of precipitation (and lows of
366 radiation) by 0-2 months (Fig. 3, Fig. S4b). In regions with a light-following relationship,
367 photosynthetic peaks lagged minimum precipitation by a wide range of 0-4 months, and
368 commonly lagged radiation peaks by 0 to 3 months, although with large variation (Fig. S4c). The
369 relatively few pixels that have the longer time lags with precipitation occur in the tropical
370 rainforests of South America, which is mostly a light-following region. A large proportion of the
371 longer time lags with radiation coincides with cosynchronous regions in the higher tropical
372 latitudes of Africa and Australia.

373   3.2 Climate properties of the different types of relationships of photosynthetic seasonality
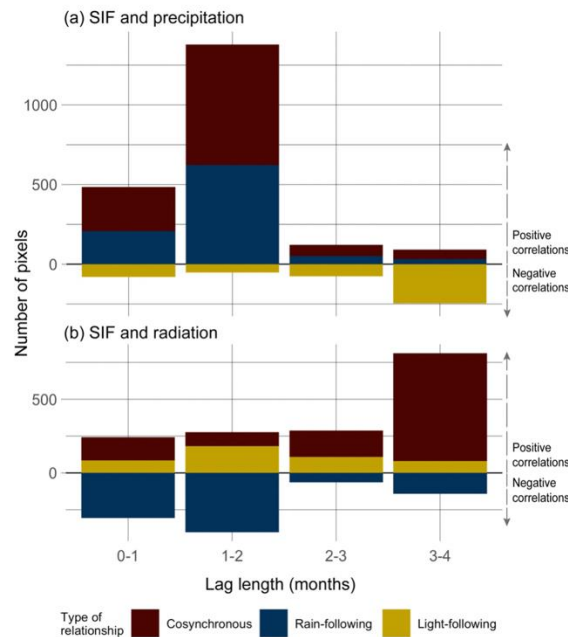374 with precipitation and radiation

375   Each of the three dominant climate-seasonality relationships was associated with distinct
376 climatic properties (Fig. 4A-E). Areas with a cosynchronous relationship tended to have
377 relatively low annual rainfall (Median = 1217 and Interquantile Range = 26 mm), high mean
378 daily radiation ($\tilde{x}$ = 227.9 and IQR = 1.12 W m^{-2}), a long dry season ($\tilde{x}$ = 221.9 and IQR = 1.4
379 days), relatively low mean temperature ($\tilde{x}$ = 25.7 and IQR = 0.1 °C), and high rainfall seasonality
380 ($\tilde{x}$ = 0.8 and IQR = 0.01). Rain-following pixels had low MAP ($\tilde{x}$ = 1214 and IQR = 24 mm),

Fig. 2. Maps of biomes and results from the CCF analysis. (Top panel): biomes of the tropics (WWF). (Other panels): Maps showing the spatial distribution of the maximum correlation coefficient from the CCF analysis for vegetation productivity from each of the datasets with precipitation and radiation. Colors in the map correspond to the colors and numbers in the reference panel Fig. 1, which contain information about the type of combined relationship and strength of the correlations. White pixels correspond to water bodies or pixels with scarce data for CCF analysis.

389   high mean daily radiation ($\tilde{x}$ = 227.9 and IQR = 0.9 W m^{-2}), an intermediate-length dry season ($\tilde{x}$
390   = 203.1 and IQR = 1.6 days), higher mean temperature ($\tilde{x}$ = 26.1 and IQR = 0.1 °C), and
391   intermediate rainfall seasonality ($\tilde{x}$ = 0.8 and IQR = 0.01). Light- following pixels had high MAP
392   ($\tilde{x}$ = 2466 and IQR = 40 mm), low mean daily radiation ($\tilde{x}$ = 201.5 and IQR = 0.7 W m^{-2}), a short
393   dry season ($\tilde{x}$ = 189.9 and IQR = 1.1 days), high mean temperature ($\tilde{x}$ = 26.4 and IQR = 0.1 °C),
394   and low precipitation seasonality ($\tilde{x}$ = 0.5 and IQR = 0.01). The climates of areas with the light-
395   following relationship stood out as distinct from those in other areas across four of the five
396   variables – only temperature, by not differing from regions with the rain-following relationship,
397   opposed this trend. Cosynchronous and rain-following pixels had similar MAP and mean daily
398   radiation, but cosynchronous pixels had a longer dry season, lower mean temperature, and larger
399   precipitation seasonality index.

400   The correlation between precipitation and radiation also provided meaningful information
401   about the relationship between photosynthetic activity and climate. In areas with a
402   cosynchronous relationship, light and precipitation typically were abundant during the same or
403   similar times of year (Fig. 4F). In these areas, photosynthesis was greatest during the times of
404   year that were both wet and bright. In contrast, in areas with the other two dominant types of
405   relationships, the rainiest times of year were the darkest, and the driest seasons were brightest. In
406   these areas, GPP responded most positively to the climate factor that was most limiting. Thus,
407   areas that have lower MAP and a longer dry are water-limited and showed a positive correlation
408   with rainfall, and consequently a negative correlation with radiation. In areas with higher MAP

409

410   **Fig. 3.** Frequency (number of pixels) of the length of lags in the strongest correlations between
411   SIF and (a) precipitation and (b) radiation for the three most common types of relationships
412   (n=2533). Colors correspond to the colors of the types of relationships shown in the reference
413   panel in Fig. 1. In order to differentiate the direction of the correlation, the count of pixels with
414   positive correlation coefficients between the climate driver and SIF is shown upward and the
415   count with negative correlation coefficients is shown downward. Note the difference in scales
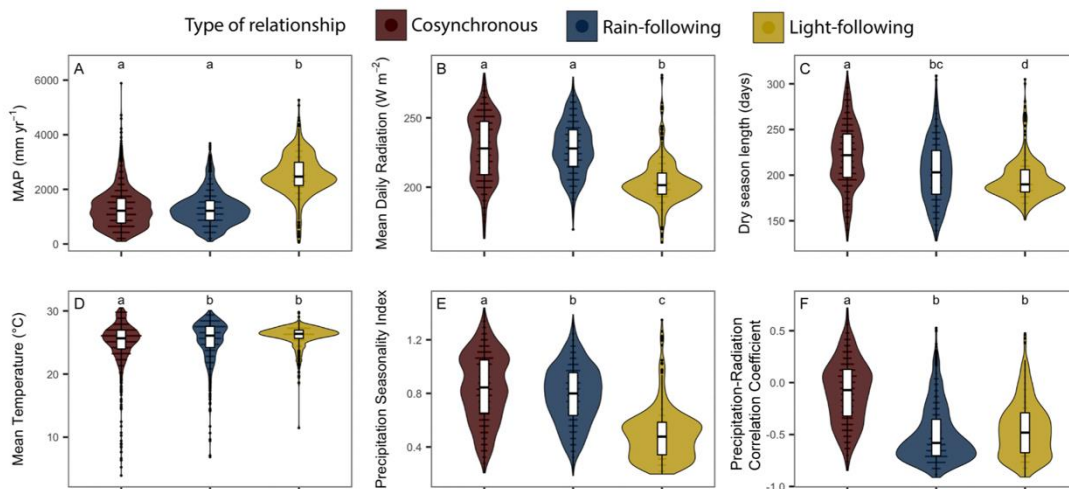416   between (a) and (b).

417 and a shorter dry season, GPP is limited by light; photosynthesis was greatest during the
418 brightest times of year and slower during the wetter (and darker) times of year.

419   3.3 Relationship of photosynthetic activity with water and light in ecosystem models

420   In land surface models, GPP showed the same three dominant types of relationships with
421 climate that we found in the satellite data. However, the proportion of vegetation with each type
422 of relationship, and the spatial distributions of these relationships, differed from observations
423 (Figs. 1, 2 and S5, S6). In the simulated data, the rain-following relationship was more
424 widespread than any other (51-53%), and always more common than in the satellite-based
425 datasets. In contrast, the proportion of cosynchronous pixels was typically lower than that shown
426 by satellite data (20-39%), as was also the case for the light-following relationship (6-11%).
427 Kappa coefficients and overall differences between the models' results and the MAIAC EVI and
428 SIF datasets (Table 1) ranged from 0.28 to 0.54 and 35.05 to 50.23%, respectively, with LPJ-
429 GUESS showing the most similarity to both satellite-based datasets. Overall, the models
430 produced more similar GPP predictions to one another than to the satellite-based observations
431 (Table 1).
432   Other vegetation products analyzed in this study also tended to show different patterns
433 from those in models and observations (Figs. 1 and 2). Fluxcom GPP had a high percentage of
434 pixels with cosynchronous and rain-following relationships (48% and 37%), while light-
435 following relationships were less common than in the satellite data (8%). VPM GPP showed a lot
436 more diversity in the type of relationships, with the greatest proportion of the tropics having
437 cosynchronous and light- following relationships (39% and 31%), and slightly less area covered
438 by rain-following pixels (25%). The Kappa coefficients and overall differences indicate that
439 VPM output agreed more closely with both satellite-based datasets and with the models than

440

Fig. 4. Climate characteristics of the three most common types of relationships inferred from
SIF. The shape of the violin plots and the horizontal lines inside of them represent number of
pixels; wider shapes and longer horizontal lines are more pixels at that level of that specific
variable. The boxplot shows the median and the quartiles. Significant differences between pairs
of groups are represented through letters; groups with same letters are not significantly different.
Colors and numbers of the types of relationships (legend) correspond to the colors and numbers
in the reference panel in Fig. 1.

448   Fluxcom (Table 1). Similar to the satellite observations, the model most similar to these two
449   GPP products was LPJ-GUESS.

450   In our biome-level comparisons (Table S2), the best agreement between SIF and most
451   models was found in montane grasslands and shrublands (κ = 0.46-0.57, D = 18-25%), flooded
452   grasslands and savannas (κ = 0.38-0.44, D = 28.6-34.2%), and grasslands and savannas (κ =
453   0.33-0.46, D = 30.7-41.8%), in that order. In contrast, low agreement was found in mangroves (κ
454   = -0.17-0.28, D = 52.2-72.7%), rainforest (κ = 0.19-0.34, D = 45.4-62.7%) and deserts and xeric
455   shrublands (κ = 0.12-0.33, D = 31.5-41.5%). In dry forests, Fluxcom and VPM showed closer
456   agreement with SIF than the land surface models did.

4 Discussion

458   Our results identify three primary relationships between photosynthetic activity and
459   seasonal patterns of water and light availability across the entire tropical region. In addition to
460   mapping these patterns, our classification provides a clear scheme for model comparison.
461   Finally, the analysis shows where, and for which climate variables, lagged correlations occur and
462   need to be accounted for in ecosystem models.

463   Previous research has shown the importance and the spatial distribution of water and light
464   as drivers of photosynthetic activity at the seasonal scale in the tropics (Guan et al., 2015;
465   Nemani et al., 2003; Seddon et al., 2016). Our results are in agreement with those studies; we
466   found the prevalence of positive correlations (1) with water in most of the drier regions in the
467   tropics and (2) with light in the wet tropical forests. In addition to finding these positive
468   correlations, we also considered negative correlations with each driver as part of our analyses.
469   These results revealed that a positive correlation with one driver does not necessarily imply a
470   negative correlation with the other driver, particularly when both climate variables are highly
471   correlated with each other. In fact, positive correlations with both drivers, a cosynchronous
472   relationship, is the most common type of relationship in the tropics.

473   The cosynchronous relationship is mainly found in regions with a low MAP, high mean
474   daily radiation, long dry season, and high precipitation seasonality. These regions correspond to
475   water-limited biomes located in higher latitudes where precipitation and radiation are not
476   negatively correlated, meaning water and light are abundant at approximately the same time.
477   Rain-following relationships are found in regions with similar precipitation and radiation
478   characteristics and are also common in similar biomes. However, this relationship is more
479   common at lower latitudes where precipitation and radiation are negatively correlated.
480   Vegetation from cosynchronous and rain-following regions is likely water-stressed for part of the
481   year, and therefore responds positively to water availability. What differentiates the regions with
482   these two types of relationships is the timing of radiation with respect to precipitation. In the
483   cosynchronous relationship, vegetation is adapted to take advantage of seasonal availability (up
484   to 4 months) of both water and light. In the rain-following relationship, vegetation is adapted to
485   periods of increased rainfall that do not coincide with the most abundant light.

486   The third most common type of relationship, the light-following relationship, is found in
487   regions with high MAP, low mean daily radiation, a short dry season, low precipitation
488   seasonality, and a negative correlation between precipitation and radiation. This relationship and
489   climate characteristics are very specific to the rainforests of South America where previous field
490   (Restrepo-Coupe et al., 2013; Saleska et al., 2003) and satellite (Bertani et al., 2017; Bradley et

491 al., 2011b; Wagner et al., 2017) findings show light-driven seasonal photosynthetic activity.
492 Similarly, the spatial distributions of the rain- and light- following relationships found here are
493 comparable to the wet- and dry-season greening regions for tropical rainforests, with those
494 forests in the central Amazon and southeast Asia greening in the dry season, when radiation
495 peaks (Doughty et al., 2019; Guan et al., 2015).

496   The mechanisms by which plant species have adapted to (or been selected by) seasonal
497 fluctuations in precipitation and light could determine vegetation responses to any future changes
498 in these patterns. Recognizing the specific correlation of photosynthetic activity in these regions
499 with the availability of water and light may lead to studies that identify relevant adaptive traits
500 and selective processes, and to better-informed predictions.

501   Rather than establishing direct causality between water, light, and photosynthetic activity,
502 we explored the nature of observed relationships. The widespread lagged correlations identified
503 here should guide experimental and mechanistic representation of photosynthetic activity. These
504 lagged correlations are consistent with analyses of Bradley et al. (2011) and Wu et al. (2015).
505 The observed time lags suggest that responses of vegetation to rain and light are influenced by
506 intermediate or indirect processes. Enhanced vegetation growth and leaf development may
507 continue long after after the seasonal peaks in delivery of water or light, such that the ecosystem
508 reaches maximum biomass of leaves, or of the most photosynthetically-efficient leaves, later in
509 the season (Duff et al., 1997; Rivera et al., 2002; J. Wu et al., 2016). This continued growth
510 could cause delayed peaks in photosynthetic activity relative to resource delivery. We found a
511 high frequency of lagged correlations in cosynchronous regions, where correlations with
512 precipitation were strongest for short time lags, but correlations with radiation tended to be
513 strongest after longer lags. The longer radiation lags mostly occur in the higher tropical latitudes.
514 We speculate that this delayed correlation is the result of plant growth and leaf development
515 continuing throughout the summer season (i.e., continuing after peak radiation), with increased
516 precipitation later in the season leading to a spike in photosynthetic activity. However,
517 phenology and increase in foliage can be highly variable in tropical ecosystems, even within the
518 same biome (Bie et al., 1998; Guan et al., 2013; Ma et al., 2013; Monasterio & Sarmiento, 1976;
519 Moore et al., 2018). Particularly in savannas, phenology and vegetation growth are influenced by
520 plant composition (i.e., tree and grass fraction covers) and fire seasonality (Guan et al., 2014;
521 Williams et al., 2005).

522   The light-following relationship is common in tropical forests, where trees have been
523 shown to increase photosynthetic activity throughout the dry season. This decoupling of
524 photosynthesis from precipitation is made possible by the deep-rooted trees, which can obtain
525 water from deep soil layers when shallow soils are dry (Nepstad et al., 1994; Restrepo-Coupe et
526 al., 2013). Thus, soil water storage and adaptive leaf development and demography likely
527 regulate the relationship between precipitation and photosynthetic activity in these regions. Both
528 mechanisms have previously been demonstrated to mediate the relationship between climate and
529 photosynthetic activity in tropical forests (Guan et al., 2015; Restrepo-Coupe et al., 2013; Wu et
530 al., 2016, 2017), and likely play a strong role in our results. For instance, some of these forests'
531 photosynthetic activity peaks happen in the late dry season, months after precipitation declined;
532 similarly, they reach low photosynthetic activity levels in the late wet season months after
533 precipitation has peaked. However, site-specific differences in variables such as soil texture and
534 plant traits also likely contribute to the observed geographical variation in these time lags. Our
535 results suggest that it is important for models to consider mechanisms such as these, which can

536 affect the relationships of tropical ecosystems' photosynthetic activity with precipitation and
537 light. Our results show the extent of the area of different types of relationships and the associated
538 time lags with each driver.

539   In general, land surface models accurately represent most of the regional variation in the
540 type of relationship of photosynthesis with precipitation and radiation. However, the models
541 have two primary deficiencies: they tend to overestimate the extent of positive relationships with
542 precipitation, and underestimate the extent of positive relationships with radiation. These two
543 issues result in models overestimating the number of rain-following pixels and underestimating
544 the number of cosynchronous and light-following pixels. Differences between models and SIF
545 results for the cosynchronous relationships are located in scattered regions and biomes across the
546 tropics, with one focus area in mainland Southeast Asia. This constitutes a highly deforested
547 region widely covered by irrigated crops (Sen et al., 2013). The differences between models and
548 remote sensing found in this region could therefore be due to the lack of representation of land
549 cover change in the simulations analyzed here.

550 **Table 1.** Kappa coefficients (κ) and overall difference (D) between the maps resulting from the
551 CCF analysis (Fig. 2). Larger $\boldsymbol{\kappa}$ values indicate closer agreement between the results of two
552 datasets. Larger D values indicate larger differences between the results of two datasets.

	MAIAC EVI	CLM4.5	JULES	LPJ-GUESS	FLUXCOM	VPM
SIF	$\kappa = 0.5$	0.28	0.3	0.39	0.4	0.48
	$D = 35.12$	50.23	49.31	43.16	41.15	37.26
MAIAC EVI		0.45	0.45	0.55	0.5	0.55
		35.05	35.31	29.02	31.96	31.24
CLM4.5			0.52	0.54	0.44	0.31
			28.2	29.03	34.81	49.2
JULES				0.55	0.4	0.32
				28.42	38.6	48.18
LPJ-GUESS					0.43	0.47
					36.42	36.6
FLUXCOM						0.43
						39.01

553   The largest differences between SIF and models are in rainforest regions. Model
554 misrepresentation of the seasonality of photosynthetic activity was previously demonstrated
555 using GPP data from eddy flux towers in the Amazon (Restrepo-Coupe et al., 2017). Our results
556 show the extent of this misrepresentation across the entire Amazon and other smaller rainforest
557 areas in Asia. The misrepresentation of rainforests, one of the largest biomes in the tropics, and
558 their characteristic light-following relationship is of major concern. As mentioned above,
559 incorporating increased rooting depth, leaf demography, or other processes could improve the
560 representation of seasonality in simulations (Poulter et al., 2009; J. Wu et al., 2017). The VPM
561 GPP dataset was able to reproduce the light-following relationship, something that neither the
562 models nor Fluxcom GPP did. VPM's capacity to represent this type of relationship might be
563 associated with the light-based model it uses to estimate GPP, which is not used by the other
564 datasets analyzed in this study. This light-use efficiency (LUE) GPP type of model not only

565 gives high importance to radiation but also uses EVI to calculate the fraction of PAR absorbed
566 by chlorophyll, which helps to improve the representation of the seasonal variation of
567 photosynthetic capacity (Zhang et al., 2017). Among the three models and the two global GPP
568 datasets studied, LPJ-GUESS and VPM showed the closest agreement with our satellite-based
569 results.

570   Land cover change has undoubtedly influenced the types of relationships observed in SIF
571 and MAIAC EVI. The model output analyzed here uses a static land cover type and could,
572 therefore, misrepresent some of the observed dynamics between climate and SIF and MAIAC
573 EVI. Therefore, we recommend a careful reading of our comparison in regions with high levels
574 of land cover change.

575   We identified clear, distinct patterns at large spatial and temporal scales in the observed
576 relationships of tropical photosynthetic activity with precipitation and radiation, despite wide
577 physiological, microclimatic and ecological variation. The large-scale nature of this study, at
578 relatively low resolution, necessarily ignores important ecological factors and confounding
579 variables associated with both climate and photosynthetic activity. Nutrient availability,
580 microclimate, topography, soil texture, plant community dynamics, and anthropogenic
581 disturbances are all important factors that influence photosynthetic activity and are not
582 considered here. Yet, the broad spatial patterns identified here can guide research on the
583 predominant mechanistic processes driving photosynthetic activity. Our evaluation of model and
584 GPP products revealed the types of climate-vegetation relationships that are least accurately
585 simulated by models. We expect that our classification of photosynthetic activity relationships
586 will simplify model comparison and benchmarking for tropical ecosystems. Our characterization
587 of the time lags shows the existence and extent of important delayed relationships of
588 photosynthetic activity with each of the climate drivers in specific vegetation types and regions
589 in the tropics. These results should guide modeling and experimental studies about the potential
590 processes that determine seasonality of photosynthetic activity in the tropics. We believe this
591 improved understanding could lead to more realistic predictions of how tropical vegetation will
592 respond to ongoing climate change, with implications for the climate system.

Data Availability Statement

600 Rainfall (TRMM, 2011) and radiation (Loeb et al., 2009) data were downloaded from GES DISC
601 (https://disc.gsfc.nasa.gov/). Temperature data is available through Harris et al. (2014) and can
602 be downloaded from CRU (https://crudata.uea.ac.uk/cru/data/hrg/). The Rainy and Dry Seasons
603 (RADS) dataset is available through Bombardi et al. (2019). SIF data were downloaded from the
604 GDFC data center (https://avdc.gsfc.nasa.gov/pub/data/satellite/MetOp/GOME_F/). The GOSIF
605 dataset is available through Li and Xiao (2019) and can be downloaded from the Global Ecology
606 Group repository (http://data.globalecology.unh.edu/data/GOSIF/). MAIAC EVI data are
607 available through Lyapustin et al. (2018) and can be downloaded from the NCCS Dataportal

608 (https://portal.nccs.nasa.gov/datashare/maiac/DataRelease/Global-VI-8day-0.05degree/). Model
609 output from the TRENDY project is available through Sitch et al. (2015).

References

611 Bertani, G., Wagner, F. H., Anderson, L. O., & Aragão, L. E. O. C. (2017). Chlorophyll
612   Fluorescence Data Reveals Climate-Related Photosynthesis Seasonality in Amazonian
613   Forests. *Remote Sensing*, *9*(12), 1275. https://doi.org/10.3390/rs9121275

614 Best, M. J., Pryor, M., Clark, D. B., Rooney, G. G., Essery, R. L. H., Ménard, C. B., Edwards, J.
615   M., Hendry, M. A., Porson, A., Gedney, N., Mercado, L. M., Sitch, S., Blyth, E.,
616   Boucher, O., Cox, P. M., Grimmond, C. S. B., & Harding, R. J. (2011). The Joint UK
617   Land Environment Simulator (JULES), model description – Part 1: Energy and water
618   fluxes. *Geoscientific Model Development*, *4*(3), 677–699. https://doi.org/10.5194/gmd-4-
619   677-2011

620 Bie, S. D., Ketner, P., Paasse, M., & Geerling, C. (1998). Woody plant phenology in the West
621   Africa savanna. *Journal of Biogeography*, *25*(5), 883–900.
622   https://doi.org/10.1046/j.1365-2699.1998.00229.x

623 Bombardi, R. J., Kinter, J. L., & Frauenfeld, O. W. (2019). A Global Gridded Dataset of the
624   Characteristics of the Rainy and Dry Seasons. *Bulletin of the American Meteorological*
625   *Society*. https://doi.org/10.1175/BAMS-D-18-0177.1

626 Box, G. E. P., Jenkins, G. M., Reinsel, G. C., Ljung, G. M., & Ljung, G. M. (2015). *Time Series*
627   *Analysis: Forecasting and Control*. John Wiley & Sons, Incorporated.
628   http://ebookcentral.proquest.com/lib/purdue/detail.action?docID=2064681

629 Bradley, A. V., Gerard, F. F., Barbier, N., Weedon, G. P., Anderson, L. O., Huntingford, C.,
630   Aragão, L. E. O. C., Zelazowski, P., & Arai, E. (2011a). Relationships between
631   phenology, radiation and precipitation in the Amazon region. *Global Change Biology*,
632   *17*(6), 2245–2260. https://doi.org/10.1111/j.1365-2486.2011.02405.x

633 Bradley, A. V., Gerard, F. F., Barbier, N., Weedon, G. P., Anderson, L. O., Huntingford, C.,
634   Aragão, L. E. O. C., Zelazowski, P., & Arai, E. (2011b). Relationships between
635   phenology, radiation and precipitation in the Amazon region. *Global Change Biology*,
636   *17*(6), 2245–2260. https://doi.org/10.1111/j.1365-2486.2011.02405.x

637 Chan, K.-S., & Ripley, B. (2012). *TSA: Time Series Analysis. R package version 1.01*.
638   https://CRAN.R-project.org/package=TSA

639 Cohen, J. (1960). A Coefficient of Agreement for Nominal Scales. *Educational and*
640   *Psychological Measurement*, *20*(1), 37–46. https://doi.org/10.1177/001316446002000104

641 Cryer, J. D., & Chan, K.-S. (2008). *Time Series Analysis: With Applications in R* (2nd ed.).
642   Springer-Verlag. https://doi.org/10.1007/978-0-387-75959-3

643 Doughty, R., Köhler, P., Frankenberg, C., Magney, T. S., Xiao, X., Qin, Y., Wu, X., & Moore,
644   B. (2019). TROPOMI reveals dry-season increase of solar-induced chlorophyll
645   fluorescence in the Amazon forest. *Proceedings of the National Academy of Sciences*,
646   *116*(44), 22393–22398. https://doi.org/10.1073/pnas.1908157116

647 Duff, G. A., Myers, B. A., Williams, R. J., Eamus, D., O'Grady, A., & Fordyce, I. R. (1997).
648   Seasonal Patterns in Soil Moisture, Vapour Pressure Deficit, Tree Canopy Cover and Pre-
649   dawn Water Potential in a Northern Australian Savanna. *Australian Journal of Botany*,
650   *45*(2), 211–224. https://doi.org/10.1071/bt96018

651 Dunn, O. J. (1964). Multiple Comparisons Using Rank Sums. *Technometrics*, *6*(3), 241–252.
652   JSTOR. https://doi.org/10.2307/1266041

Guan, K., Pan, M., Li, H., Wolf, A., Wu, J., Medvigy, D., Caylor, K. K., Sheffield, J., Wood, E. F., Malhi, Y., Liang, M., Kimball, J. S., Saleska, S. R., Berry, J., Joiner, J., & Lyapustin, A. I. (2015). Photosynthetic seasonality of global tropical forests constrained by hydroclimate. *Nature Geoscience*, *8*(4), 284–289. https://doi.org/10.1038/ngeo2382

Guan, K., Wolf, A., Medvigy, D., Caylor, K. K., Pan, M., & Wood, E. F. (2013). Seasonal coupling of canopy structure and function in African tropical forests and its environmental controls. *Ecosphere*, *4*(3), art35. https://doi.org/10.1890/ES12-00232.1

Guan, K., Wood, E. F., Medvigy, D., Kimball, J., Pan, M., Caylor, K. K., Sheffield, J., Xu, X., & Jones, M. O. (2014). Terrestrial hydrological controls on land surface phenology of African savannas and woodlands. *Journal of Geophysical Research: Biogeosciences*, *119*(8), 1652–1669. https://doi.org/10.1002/2013JG002572

Hansen, M. C., Potapov, P. V., Moore, R., Hancher, M., Turubanova, S. A., Tyukavina, A., Thau, D., Stehman, S. V., Goetz, S. J., Loveland, T. R., Kommareddy, A., Egorov, A., Chini, L., Justice, C. O., & Townshend, J. R. G. (2013). High-Resolution Global Maps of 21st-Century Forest Cover Change. *Science*, *342*(6160), 850–853. https://doi.org/10.1126/science.1244693

Harris, I., Jones, P. D., Osborn, T. J., & Lister, D. H. (2014). Updated high-resolution grids of monthly climatic observations – the CRU TS3.10 Dataset. *International Journal of Climatology*, *34*(3), 623–642. https://doi.org/10.1002/joc.3711

Huete, A. R., Didan, K., Shimabukuro, Y. E., Ratana, P., Saleska, S. R., Hutyra, L. R., Yang, W., Nemani, R. R., & Myneni, R. (2006). Amazon rainforests green-up with sunlight in dry season. *Geophysical Research Letters*, *33*(6). https://doi.org/10.1029/2005GL025583

Huffman, G. J., Bolvin, D. T., Nelkin, E. J., Wolff, D. B., Adler, R. F., Gu, G., Hong, Y., Bowman, K. P., & Stocker, E. F. (2007). The TRMM Multisatellite Precipitation Analysis (TMPA): Quasi-Global, Multiyear, Combined-Sensor Precipitation Estimates at Fine Scales. *Journal of Hydrometeorology*, *8*(1), 38–55. https://doi.org/10.1175/JHM560.1

Hyndman, R. (2017). *_forecast: Forecasting functions for time series and linear models_. R package version 8.2*. http://pkg.robjhyndman.com/forecast

Joiner, J., Guanter, L., Lindstrot, R., Voigt, M., Vasilkov, A. P., Middleton, E. M., Huemmrich, K. F., Yoshida, Y., & Frankenberg, C. (2013). Global monitoring of terrestrial chlorophyll fluorescence from moderate-spectral-resolution near-infrared satellite measurements: Methodology, simulations, and application to GOME-2. *Atmospheric Measurement Techniques*, *6*(10), 2803–2823. https://doi.org/10.5194/amt-6-2803-2013

Joiner, J., Yoshida, Y., Vasilkov, A. P., Schaefer, K., Jung, M., Guanter, L., Zhang, Y., Garrity, S., Middleton, E. M., Huemmrich, K. F., Gu, L., & Belelli Marchesini, L. (2014). The seasonal cycle of satellite chlorophyll fluorescence observations and its relationship to vegetation phenology and ecosystem atmosphere carbon exchange. *Remote Sensing of Environment*, *152*, 375–391. https://doi.org/10.1016/j.rse.2014.06.022

Joiner, J., Yoshida, Y., Vasilkov, A. P., Yoshida, Y., Corp, L. A., & Middleton, E. M. (2011). First observations of global and seasonal terrestrial chlorophyll fluorescence from space. *Biogeosciences*, *8*(3), 637–651. https://doi.org/10.5194/bg-8-637-2011

Jung, M., & Team, F. (2016). *FLUXCOM (RS+METEO) Global Land Carbon Fluxes using CRUNCEP climate data* [Data set]. https://doi.org/10.17871/fluxcom_rs_meteo_cruncepv6_1980_2013_v1

698 Kato, S., Loeb, N. G., Rose, F. G., Doelling, D. R., Rutan, D. A., Caldwell, T. E., Yu, L., &
699   Weller, R. A. (2013). Surface Irradiances Consistent with CERES-Derived Top-of-
700   Atmosphere Shortwave and Longwave Irradiances. *Journal of Climate*, *26*(9), 2719–
701   2740. https://doi.org/10.1175/JCLI-D-12-00436.1
702 Kruskal, W. H., & Wallis, W. A. (1952). Use of Ranks in One-Criterion Variance Analysis.
703   *Journal of the American Statistical Association*, *47*(260), 583–621. JSTOR.
704   https://doi.org/10.2307/2280779
705 Lawrence, D., & Vandecar, K. (2015). Effects of tropical deforestation on climate and
706   agriculture. *Nature Climate Change*, *5*(1), 27–36. https://doi.org/10.1038/nclimate2430
707 Li, X., & Xiao, J. (2019). A Global, 0.05-Degree Product of Solar-Induced Chlorophyll
708   Fluorescence Derived from OCO-2, MODIS, and Reanalysis Data. *Remote Sensing*,
709   *11*(5), 517. https://doi.org/10.3390/rs11050517
710 Loeb, N. G., B. A. Wielicki, D. R. Doelling, G. L. Smith, D. F. Keyes, S. Kato, N. Manalo-
711   Smith, T. Wong, 2009: Toward optimal closure of the Earth's top-of-atmosphere
712   radiation budget. J . Climate, 22, 748-766, doi:10.1175/2008JCLI2637.1.
713 Lyapustin, A. I., Wang, Y., Laszlo, I., Hilker, T., G.Hall, F., Sellers, P. J., Tucker, C. J., &
714   Korkin, S. V. (2012). Multi-angle implementation of atmospheric correction for MODIS
715   (MAIAC): 3. Atmospheric correction. *Remote Sensing of Environment*, *127*, 385–393.
716   https://doi.org/10.1016/j.rse.2012.09.002
717 Lyapustin, A., Wang, Y., Korkin, S., & Huang, D. (2018). MODIS Collection 6 MAIAC
718   algorithm. *Atmospheric Measurement Techniques*, *11*(10), 5741–5765.
719   https://doi.org/10.5194/amt-11-5741-2018
720 Ma, X., Huete, A., Yu, Q., Coupe, N. R., Davies, K., Broich, M., Ratana, P., Beringer, J., Hutley,
721   L. B., Cleverly, J., Boulain, N., & Eamus, D. (2013). Spatial patterns and temporal
722   dynamics in savanna vegetation phenology across the North Australian Tropical
723   Transect. *Remote Sensing of Environment*, *139*, 97–115.
724   https://doi.org/10.1016/j.rse.2013.07.030
725 Maeda, E. E., Moura, Y. M., Wagner, F., Hilker, T., Lyapustin, A. I., Wang, Y., Chave, J.,
726   Mõttus, M., Aragão, L. E. O. C., & Shimabukuro, Y. (2016). Consistency of vegetation
727   index seasonality across the Amazon rainforest. *International Journal of Applied Earth
728   Observation and Geoinformation*, *52*, 42–53. https://doi.org/10.1016/j.jag.2016.05.005
729 Malhi, Y., Roberts, J. T., Betts, R. A., Killeen, T. J., Li, W., & Nobre, C. A. (2008). Climate
730   Change, Deforestation, and the Fate of the Amazon. *Science*, *319*(5860), 169–172.
731   https://doi.org/10.1126/science.1146961
732 Mitchard, E. T. A. (2018). The tropical forest carbon cycle and climate change. *Nature*,
733   *559*(7715), 527. https://doi.org/10.1038/s41586-018-0300-2
734 Monasterio, M., & Sarmiento, G. (1976). Phenological Strategies of Plant Species in the Tropical
735   Savanna and the Semi-Deciduous Forest of the Venezuelan Llanos. *Journal of
736   Biogeography*, *3*(4), 325–355. JSTOR. https://doi.org/10.2307/3037976
737 Moore, C. E., Beringer, J., Donohue, R. J., Evans, B., Exbrayat, J.-F., Hutley, L. B., & Tapper,
738   N. J. (2018). Seasonal, interannual and decadal drivers of tree and grass productivity in
739   an Australian tropical savanna. *Global Change Biology*, *24*(6), 2530–2544.
740   https://doi.org/10.1111/gcb.14072
741 Myneni, R. B., Yang, W., Nemani, R. R., Huete, A. R., Dickinson, R. E., Knyazikhin, Y., Didan,
742   K., Fu, R., Juárez, R. I. N., Saatchi, S. S., Hashimoto, H., Ichii, K., Shabanov, N. V., Tan,
743   B., Ratana, P., Privette, J. L., Morisette, J. T., Vermote, E. F., Roy, D. P., … Salomonson,

V. V. (2007). Large seasonal swings in leaf area of Amazon rainforests. *Proceedings of the National Academy of Sciences*, *104*(12), 4820–4823. https://doi.org/10.1073/pnas.0611338104

Nemani, R. R., Keeling, C. D., Hashimoto, H., Jolly, W. M., Piper, S. C., Tucker, C. J., Myneni, R. B., & Running, S. W. (2003). Climate-Driven Increases in Global Terrestrial Net Primary Production from 1982 to 1999. *Science*, *300*(5625), 1560–1563. https://doi.org/10.1126/science.1082750

Nepstad, D. C., de Carvalho, C. R., Davidson, E. A., Jipp, P. H., Lefebvre, P. A., Negreiros, G. H., da Silva, E. D., Stone, T. A., Trumbore, S. E., & Vieira, S. (1994). The role of deep roots in the hydrological and carbon cycles of Amazonian forests and pastures. *Nature*, *372*(6507), 666–669.

Ogle, D. H., Wheeler, P., & Dinno, A. (2018). *FSA: Fisheries Stock Analysis. R package version 0.8.22*. https://github.com/droglenc/FSA

Oleson, K., Lawrence, M., Bonan, B., Drewniak, B., Huang, M., Koven, D., Levis, S., Li, F., Riley, J., Subin, M., Swenson, S., Thornton, E., Bozbiyik, A., Fisher, R., Heald, L., Kluzek, E., Lamarque, J.-F., Lawrence, J., Leung, R., … Yang, Z.-L. (2013). *Technical description of version 4.5 of the Community Land Model (CLM)*. https://doi.org/10.5065/D6RR1W7M

Pontius Jr., R. G., & Santacruz, A. (2019). *DiffeR: Metrics of Difference for Comparing Pairs of Maps or Pairs of Variables* (R package version 0.0-6) [Computer software]. https://CRAN.R-project.org/package=diffeR

Pontius, R. G., & Santacruz, A. (2014). Quantity, exchange, and shift components of difference in a square contingency table. *International Journal of Remote Sensing*, *35*(21), 7543–7554. https://doi.org/10.1080/2150704X.2014.969814

Poulter, B., Heyder, U., & Cramer, W. (2009). Modeling the Sensitivity of the Seasonal Cycle of GPP to Dynamic LAI and Soil Depths in Tropical Rainforests. *Ecosystems*, *12*(4), 517–533. https://doi.org/10.1007/s10021-009-9238-4

Probst, W. N., Stelzenmüller, V., & Fock, H. O. (2012). Using cross-correlations to assess the relationship between time-lagged pressure and state indicators: An exemplary analysis of North Sea fish population indicators. *ICES Journal of Marine Science*, *69*(4), 670–681. https://doi.org/10.1093/icesjms/fss015

R Core Team. (2017). *R: A language and environment for statistical computing.* R Foundation for Statistical Computing, Vienna, Austria. https://www.R-project.org/

Restrepo-Coupe, N., da Rocha, H. R., Hutyra, L. R., da Araujo, A. C., Borma, L. S., Christoffersen, B., Cabral, O. M. R., de Camargo, P. B., Cardoso, F. L., da Costa, A. C. L., Fitzjarrald, D. R., Goulden, M. L., Kruijt, B., Maia, J. M. F., Malhi, Y. S., Manzi, A. O., Miller, S. D., Nobre, A. D., von Randow, C., … Saleska, S. R. (2013). What drives the seasonality of photosynthesis across the Amazon basin? A cross-site analysis of eddy flux tower measurements from the Brasil flux network. *Agricultural and Forest Meteorology*, *182–183*, 128–144. https://doi.org/10.1016/j.agrformet.2013.04.031

Restrepo-Coupe, N., Levine, N. M., Christoffersen, B. O., Albert, L. P., Wu, J., Costa, M. H., Galbraith, D., Imbuzeiro, H., Martins, G., Araujo, A. C. da, Malhi, Y. S., Zeng, X., Moorcroft, P., & Saleska, S. R. (2017). Do dynamic global vegetation models capture the seasonality of carbon fluxes in the Amazon basin? A data-model intercomparison. *Global Change Biology*, *23*(1), 191–208. https://doi.org/10.1111/gcb.13442

Rivera, G., Elliott, S., Caldas, L. S., Nicolossi, G., Coradin, V. T., & Borchert, R. (2002). Increasing day-length induces spring flushing of tropical dry forest trees in the absence of rain. *Trees*, *16*(7), 445–456. https://doi.org/10.1007/s00468-002-0185-3

Saigusa, N., Yamamoto, S., Hirata, R., Ohtani, Y., Ide, R., Asanuma, J., Gamo, M., Hirano, T., Kondo, H., Kosugi, Y., Li, S.-G., Nakai, Y., Takagi, K., Tani, M., & Wang, H. (2008). Temporal and spatial variations in the seasonal patterns of CO2 flux in boreal, temperate, and tropical forests in East Asia. *Agricultural and Forest Meteorology*, *148*(5), 700–713. https://doi.org/10.1016/j.agrformet.2007.12.006

Saleska, S. R., Miller, S. D., Matross, D. M., Goulden, M. L., Wofsy, S. C., da Rocha, H. R., de Camargo, P. B., Crill, P., Daube, B. C., de Freitas, H. C., Hutyra, L., Keller, M., Kirchhoff, V., Menton, M., Munger, J. W., Pyle, E. H., Rice, A. H., & Silva, H. (2003). Carbon in Amazon Forests: Unexpected Seasonal Fluxes and Disturbance-Induced Losses. *Science*, *302*(5650), 1554–1557. JSTOR.

Seddon, A. W. R., Macias-Fauria, M., Long, P. R., Benz, D., & Willis, K. J. (2016). Sensitivity of global terrestrial ecosystems to climate variability. *Nature*, *531*(7593), 229–232. https://doi.org/10.1038/nature16986

Sen, O. L., Bozkurt, D., Vogler, J. B., Fox, J., Giambelluca, T. W., & Ziegler, A. D. (2013). Hydro-climatic effects of future land-cover/land-use change in montane mainland southeast Asia. *Climatic Change; Dordrecht*, *118*(2), 213–226. http://dx.doi.org.ezproxy.lib.purdue.edu/10.1007/s10584-012-0632-0

Sitch, S., Friedlingstein, P., Gruber, N., Jones, S. D., Murray-Tortarolo, G., Ahlström, A., Doney, S. C., Graven, H., Heinze, C., Huntingford, C., Levis, S., Levy, P. E., Lomas, M., Poulter, B., Viovy, N., Zaehle, S., Zeng, N., Arneth, A., Bonan, G., … Myneni, R. (2015). Recent trends and drivers of regional sources and sinks of carbon dioxide. *Biogeosciences*, *12*(3), 653–679. https://doi.org/10.5194/bg-12-653-2015

Smith, B., Prentice, I. C., & Sykes, M. T. (2001). Representation of Vegetation Dynamics in the Modelling of Terrestrial Ecosystems: Comparing Two Contrasting Approaches within European Climate Space. *Global Ecology and Biogeography*, *10*(6), 621–637. JSTOR.

Tramontana, G., Jung, M., Schwalm, C. R., Ichii, K., Camps-Valls, G., Ráduly, B., Reichstein, M., Arain, M. A., Cescatti, A., Kiely, G., Merbold, L., Serrano-Ortiz, P., Sickert, S., Wolf, S., & Papale, D. (2016). Predicting carbon dioxide and energy fluxes across global FLUXNET sites with regression algorithms. *Biogeosciences*, *13*(14), 4291–4313. https://doi.org/10.5194/bg-13-4291-2016

Tropical Rainfall Measuring Mission (TRMM) (2011), TRMM (TMPA/3B43) Rainfall Estimate L3 1 month 0.25 degree x 0.25 degree V7, Greenbelt, MD, Goddard Earth Sciences Data and Information Services Center (GES DISC), Accessed February 2018, 10.5067/TRMM/TMPA/MONTH/7

Wagner, F. H., Hérault, B., Rossi, V., Hilker, T., Maeda, E. E., Sanchez, A., Lyapustin, A. I., Galvão, L. S., Wang, Y., & Aragão, L. E. O. C. (2017). Climate drivers of the Amazon forest greening. *PLOS ONE*, *12*(7), e0180932. https://doi.org/10.1371/journal.pone.0180932

Walsh, R. P. D., & Lawler, D. M. (1981). Rainfall Seasonality: Description, Spatial Patterns and Change Through Time. *Weather*, *36*(7), 201–208. https://doi.org/10.1002/j.1477-8696.1981.tb05400.x

833   Williams, P. R., Congdon, R. A., Grice, A. C., & Clarke, P. J. (2005). Germinable soil seed
834   banks in a tropical savanna: Seasonal dynamics and effects of fire. *Austral Ecology*,
835   *30*(1), 79–90. https://doi.org/10.1111/j.1442-9993.2004.01426.x
836   Wu, D., Zhao, X., Liang, S., Zhou, T., Huang, K., Tang, B., & Zhao, W. (2015). Time-lag effects
837   of global vegetation responses to climate change. *Global Change Biology*, *21*(9), 3520–
838   3531. https://doi.org/10.1111/gcb.12945
839   Wu, J., Albert, L. P., Lopes, A. P., Restrepo-Coupe, N., Hayek, M., Wiedemann, K. T., Guan,
840   K., Stark, S. C., Christoffersen, B., Prohaska, N., Tavares, J. V., Marostica, S.,
841   Kobayashi, H., Ferreira, M. L., Campos, K. S., Silva, R. da, Brando, P. M., Dye, D. G.,
842   Huxman, T. E., … Saleska, S. R. (2016). Leaf development and demography explain
843   photosynthetic seasonality in Amazon evergreen forests. *Science*, *351*(6276), 972–976.
844   https://doi.org/10.1126/science.aad5068
845   Wu, J., Serbin, S. P., Xu, X., Albert, L. P., Chen, M., Meng, R., Saleska, S. R., & Rogers, A.
846   (2017). The phenology of leaf quality and its within-canopy variation is essential for
847   accurate modeling of photosynthesis in tropical evergreen forests. *Global Change
848   Biology*, *23*(11), 4814–4827. https://doi.org/10.1111/gcb.13725
849   Xu, L., Saatchi, S. S., Yang, Y., Myneni, R. B., Frankenberg, C., Chowdhury, D., & Bi, J.
850   (2015). Satellite observation of tropical forest seasonality: Spatial patterns of carbon
851   exchange in Amazonia. *Environmental Research Letters*, *10*(8), 084005.
852   https://doi.org/10.1088/1748-9326/10/8/084005
853   Zhang, Y., Joiner, J., Gentine, P., & Zhou, S. (2018). Reduced solar-induced chlorophyll
854   fluorescence from GOME-2 during Amazon drought caused by dataset artifacts. *Global
855   Change Biology*, *24*(6), 2229–2230. https://doi.org/10.1111/gcb.14134
856   Zhang, Y., Xiao, X., Wu, X., Zhou, S., Zhang, G., Qin, Y., & Dong, J. (2017). A global
857   moderate resolution dataset of gross primary production of vegetation for 2000–2016.
858   *Scientific Data*, *4*, 170165. https://doi.org/10.1038/sdata.2017.165

859